

# Non-Equilibrium Probing of Topological Supersolids in Spin-Orbit-Coupled Dipolar Condensates

Biao Dong,<sup>1</sup> Xiao-Fei Zhang,<sup>2,\*</sup> Wei Han,<sup>3</sup> Renyuan Liao,<sup>4,5</sup>  
Xue-Ying Yang,<sup>6</sup> Wu-Ming Liu,<sup>7,†</sup> and Yong-Chang Zhang<sup>1,‡</sup>

<sup>1</sup>*MOE Key Laboratory for Nonequilibrium Synthesis and Modulation of Condensed Matter,  
Shaanxi Key Laboratory of Quantum Information and Quantum Optoelectronic Devices,  
School of Physics, Xi'an Jiaotong University, Xi'an 710049, China*

<sup>2</sup>*Department of Physics, Shaanxi University of Science and Technology, Xi'an 710021, China*

<sup>3</sup>*State Key Laboratory of Quantum Optics Technologies and Devices,  
Institute of Opto-Electronics, Collaborative Innovation Center of Extreme Optics,  
Shanxi University, Taiyuan, Shanxi 030006, China*

<sup>4</sup>*Fujian Provincial Key Laboratory for Quantum Manipulation and New Energy Materials,  
College of Physics and Energy, Fujian Normal University, Fuzhou 350117, China*

<sup>5</sup>*Fujian Provincial Collaborative Innovation Center for Advanced High-Field  
Superconducting Materials and Engineering, Fuzhou 350117, China*

<sup>6</sup>*Key Laboratory of Time Reference and Applications,  
National Time Service Center, Chinese Academy of Sciences, Xi'an 710600, China*

<sup>7</sup>*Beijing National Laboratory for Condensed Matter Physics,  
Institute of Physics, Chinese Academy of Sciences, Beijing 100190, China*

(Dated: April 22, 2025)

A chiral supersolid is a quantum phase that simultaneously exhibits crystalline order, superfluidity, and topological spin texture, with spontaneously broken translational, U(1) gauge, and chiral symmetries. Here, we demonstrate a chiral supersolid with tunable non-equilibrium dynamics in a spin-orbit coupled dipolar Bose-Einstein condensate. By adjusting dipolar interaction and spin-orbit coupling, we uncover two distinct quantum phase transitions: (i) a first-order transition from a single skyrmion superfluid to a triangular meron supersolid, and (ii) a second-order transition from this superfluid to a square skyrmion supersolid. These phases are characterized by their lattice symmetries, nonclassical rotational inertia, and spin textures. Under parity-time symmetric dissipation, we predict phase-dependent damping of the current oscillations, directly linked to the superfluid fraction. The predicted chiral supersolid phase can be experimentally observed in ultracold magnetic atoms with spin-orbit coupling. Our results establish dipolar quantum gases as a platform for designing topological matter with spintronic functionality.

*Introduction.*—Chirality, a hallmark of symmetry breaking across scales from condensed matter [1–3] to particle physics [4, 5], underpins topological phenomena and spintronic functionalities [6–8]. Controllable chirality offers a versatile tool for exploring many-body physics and manipulating magnetic textures, with applications in information storage and data processing [9–15]. In condensed matter systems, chiral spin textures, e.g., skyrmions and merons, exhibit unique transport properties, yet their phases are often constrained by fixed lattice symmetries and weak tunability [16–26]. Ultracold atomic gases, with unparalleled control over interactions and confinement, provide a transformative platform to engineer chiral quantum matter. However, the simultaneous realization of topological spin textures, supersolidity, and non-equilibrium control, critical for topological transport and quantum simulation, remains an outstanding challenge.

Beyond topological spin textures and crystal structures, the superfluidity in cold-atom chiral states, marked by spontaneous U(1) gauge symmetry breaking, distinguishes them from conventional condensed matter systems. Superfluidity, characterized by dissipationless coherent flow, enables energy-efficient information process-

ing devices [27, 28]. Recent advances in ultracold magnetic atomic gases have unlocked long-range dipolar interactions, paving the way for emergent self-organization in superfluids, such as supersolids [29–33]. Integrating these systems with synthetic spin-orbit coupling (SOC) [34–41] offers a powerful platform to explore novel states of matter hosting simultaneous superfluid, crystalline, and topological magnetic orders. The high controllability of ultracold atoms further enables precisely manipulated transitions between chiral phases, a capability with promising applications in quantum devices but requiring further exploration.

In this Letter, we study a two-component Bose-Einstein condensate (BEC) with synthetic SOC, where dipolar interactions stabilize supersolidity while SOC generates spin textures. By tuning the SOC strength ( $\kappa$ ) and dipolar interaction ratio ( $\varepsilon_{dd}$ ) [42], we control the superfluid fraction (superfluid to supersolid) and topology (merons to skyrmions). A second-order transition to a square lattice, absent in single-component systems, emerges from vanishing cubic terms in the energy expansion, which is a mechanism unique to multicomponent dipolar gases [43]. Experimental protocols using magnetic atoms, including optical Raman dressing for

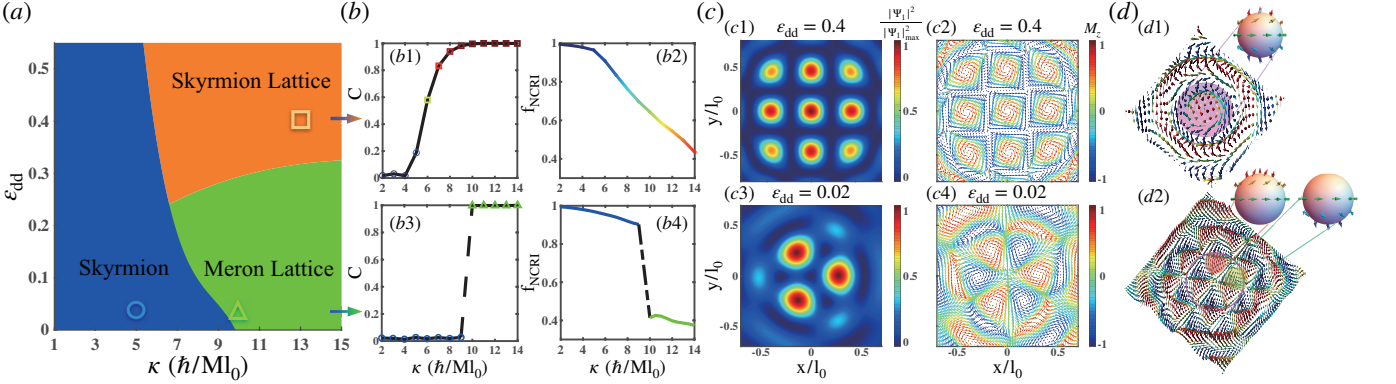


FIG. 1. (a) The phase diagram shows ground states of singly skyrmion (blue), skyrmion-type (orange), and meron-type (green) chiral supersolids (CSSs) in a spin-1/2 dipolar condensate with SOC. Contact interactions are fixed at  $g_{ij}N = g_{ii}N = gN = 0.5$ . The dipolar interaction ratio  $\varepsilon_{dd} = \frac{a_{dd}}{a}$  and SOC strength  $\kappa$  are varied. (b) Crystalline order (b1,b3) and non-classical rotational inertia fraction (NCRIF) (b2,b4) of the dipolar component evolve with  $\kappa$ , transiting from singly skyrmion to skyrmion-type (b1,b2) or meron-type (b3,b4) CSSs for strong ( $\varepsilon_{dd} = 0.4$ ) or weak ( $\varepsilon_{dd} = 0.02$ ) dipolar interactions, respectively. (c) Density profiles of the dipolar component (c1,c3) and spin textures (c2,c4) are shown for skyrmion-type CSS (c1,c2) at  $\kappa = 13$  and meron-type CSS (c3,c4) at  $\kappa = 10$ . The color in (c2,c4) represents the  $z$ -component of spin density  $M_z = \frac{1}{2}(|\Psi_1|^2 - |\Psi_2|^2)/(|\Psi_1|^2 + |\Psi_2|^2)$ . (d) Spin textures of a skyrmion (d1) and meron pair (d2) map to 3D Bloch spheres, corresponding to the singly skyrmion (or one skyrmion of the skyrmion-type CSS) and meron-type CSS phases, respectively.

SOC [35, 44–46] and Feshbach resonances for interaction tuning [47], validate feasibility. Linking equilibrium phase transitions to non-equilibrium dynamics, we establish dipolar quantum gases as a versatile platform for engineering topological matter. This work bridges condensed matter physics and atomic-scale control, opening pathways to functional spin textures for spintronics and quantum simulation.

*Theoretical model.*—We consider a two-component spin-orbit coupled BEC, where component 1 consists of magnetic dipolar atoms and component 2 is nonmagnetic [48–50]. A magnetic field aligns the dipoles, and at zero temperature, the system is described by the macroscopic wave function  $\Psi = (\Psi_1, \Psi_2)$ , governed by the Gross-Pitaevskii equation derived from the nondimensionalized mean-field energy [51, 52]

$$\mathcal{E}[\Psi_1, \Psi_2] = \int d\mathbf{r} \left\{ \sum_{j=1,2} \left[ \Psi_j^* \left( -\frac{1}{2} \nabla^2 + \frac{1}{2} r^2 \right) \Psi_j + \frac{gN}{2} |\Psi_j|^4 \right] + g_{12}N |\Psi_1|^2 |\Psi_2|^2 + \frac{g_{dd}N}{2} \Phi_{dd} |\Psi_1|^2 - i\kappa [\Psi_1^* (\partial_x - i\partial_y) \Psi_2 + \Psi_2^* (\partial_x + i\partial_y) \Psi_1] \right\}, \quad (1)$$

where  $\int d\mathbf{r} (|\Psi_1|^2 + |\Psi_2|^2) = 1$ . Here,  $\Phi_{dd}(\mathbf{r}) = 4\pi \mathcal{F}_{2D}^{-1} [\tilde{n}_1(\mathbf{k}) F(\mathbf{k}/\sqrt{2})]$ , with  $\tilde{n}_1(\mathbf{k}) = \mathcal{F}_{2D}[|\Psi_1(\mathbf{r})|^2]$  and  $F(\mathbf{k}) = 2 - 3\sqrt{\pi}ke^{k^2}\text{Erfc}(k)$ , where  $\mathcal{F}_{2D}$  is the two-dimensional Fourier transformation operator [49]. The SOC strength  $\kappa$  and dipole-dipole interaction (DDI) strength  $g_{dd} = 4\pi a_{dd}/\sqrt{2\pi}l_z$  are controlled experimentally via Raman coupling in  $^{52}\text{Cr}$  gases and magnetic Feshbach resonances, where  $l_z = \sqrt{\hbar/M\omega_z}$  and  $a_{dd} = \frac{\mu_0\mu^2 M}{12\pi\hbar^2}$  [53–55].  $\mu$  and  $\mu_0$  are the dipole moment of

the atom and the permeability of free space, respectively. We explore the parameter space with  $\kappa \in [1, 15]$  and  $\varepsilon_{dd} \equiv \frac{a_{dd}}{a} \in [0, 0.5]$ , fixing contact interactions at  $gN = 0.5$ . The intra-component contact interactions are equal  $g_{11} = g_{22} = g = 4\pi a/\sqrt{2\pi}l_z$ , with  $a$  the  $s$ -wave scattering length. Contact interactions are fixed at  $g_{ij}N = g_{ii}N = gN = 0.5$ . Energies and lengths are rescaled by  $\hbar\omega_\perp$  and  $l_0 = \sqrt{\hbar/M\omega_\perp}$ , respectively, where  $M$  is the atomic mass and  $\omega_\perp$  the radial trap frequency.

Without dipolar interactions, strengthening SOC in a weakly interacting condensate drives a phase transition from a half-quantum vortex to a hexagonal skyrmion lattice [56]. In contrast, the competition between DDI and SOC leads to phases with distinct topological and geometric properties. We numerically minimize the energy  $\mathcal{E}[\Psi_1, \Psi_2]$  in Eq. (1) and explore ground-state phases by varying the dipolar-to-contact interaction ratio  $\varepsilon_{dd} = \frac{g_{dd}}{g}$  and SOC strength [46].

*Ground-state phase diagram and spin textures.*—Fig. 1(a) summarizes our main results, showing the ground-state phase diagram as a function of SOC strength  $\kappa$  and dipolar-to-contact interaction ratio  $\varepsilon_{dd}$ . The diagram divides into two regions: a superfluid at weak SOC and a supersolid at strong SOC. For weak SOC, the condensate forms a single skyrmion without density modulation along the angle direction, characteristic of a superfluid. Beyond a critical  $\kappa_c$ , density modulation emerges, leading to crystallization and two types of chiral supersolid (CSS) states: meron and skyrmion lattices. The transition between these CSS states is controlled by  $\varepsilon_{dd}$ . For small  $\varepsilon_{dd}$  (contact-dominated regime), the ground state exhibits a triangular density distribution and meron spin textures [Fig. 1(c3) and Fig. 1(c4)],

consistent with previous predictions for spin-orbit coupled BECs [56]. Surprisingly, we also find a skyrmion supersolid with a square density profile and skyrmion spin textures [Fig. 1(c1) and Fig. 1(c2)]. Unlike single-component dipolar systems, which typically favor hexagonal structures, this square symmetry arises uniquely from the interplay of DDI and SOC.

For weak SOC ( $\kappa < \kappa_c$ ), the wave function from Eq. (1) exhibits U(1) symmetry breaking, forming a superfluid phase with a singly skyrmion state of topological charge  $Q = \pm 1$  [12]. Increasing  $\kappa$  beyond  $\kappa_c$  breaks rotational symmetry, stabilizing supersolids with triangular or square lattices depending on dipolar interaction strength [Fig. 1(a) and Fig. 1(c)]. We observe a first-order transition from superfluid to meron supersolid and, unexpectedly, a second-order transition to skyrmion supersolid.

Momentum-space densities [Fig. 3(b)] reveal the breaking of continuous rotational symmetry into three- and four-fold discrete rotational symmetries for meron and skyrmion supersolids, respectively. These phases are separated by a critical line at  $\varepsilon_{dd} \approx 0.2\text{--}0.3$  [Fig. 1(a)]. The reciprocal lattice vector  $|\mathbf{k}|$  increases (lattice constant  $a_{sky}$  decreases) with  $\kappa$ , constrained by  $\sqrt{3}|\mathbf{k}|a_{sky}/2 = 2\pi$  (triangular) and  $|\mathbf{k}|a_{sky} = 2\pi$  (square). This behavior aligns with predictions for unconfined spin-orbit coupled condensates, where the roton minimum shifts to higher momentum as  $\kappa$  increases [57–59].

The superfluid-to-supersolid transition is accompanied by dramatic changes in magnetic properties. The singly skyrmion in the superfluid phase ( $Q = \pm 1$ ) is replaced by chiral lattices of skyrmions ( $Q = 1$ ) or meron-antimeron pairs ( $Q = \pm 1/2$ ) with distinct spin textures [Fig. 1(c2) and Fig. 1(c4)]. The topology of these textures is quantified by the skyrmion number  $Q = \frac{1}{4\pi} \int d\mathbf{r} \hat{\mathbf{M}} \cdot (\frac{\partial \hat{\mathbf{M}}}{\partial x} \times \frac{\partial \hat{\mathbf{M}}}{\partial y})$ , where  $\hat{\mathbf{M}} = \Psi^\dagger (\frac{1}{2} \hat{\boldsymbol{\sigma}}) \Psi / \Psi^\dagger \Psi$  is the local magnetization on the Bloch sphere [60]. The square skyrmion lattice exhibits clockwise rotation ( $Q = 1$ ), while the triangular meron lattice features alternating meron-antimeron pairs ( $Q = \pm 1/2$ ) [Fig. 1(c4) and Fig. 1(d2)]. These phases are further distinguished by their crystalline order and NCRIF, as detailed below.

Tuning intra- and inter-component contact interactions enables precise control over density modulation and spin chirality, yielding supersolids with tailored droplet configurations and magnetic orders. Strong inter-component repulsion ( $g_{ij}N = 20$ ) drives density modulation, while intra-component interactions ( $g_{ii}N = 10$ ) stabilize a plane-wave phase with uniform spin alignment [Fig. 2(a2) and Fig. 2(a3)]. For weak intra-component interactions ( $g_{ii}N = 0.5$ ), chiral spin textures emerge at a critical balance: SOC promotes stripe phase, stabilizing a spin density wave, while dipolar interactions ( $\varepsilon_{dd} = 0.02$  or  $\varepsilon_{dd} = 0.4$ ) reinforce triangular or square lattice structures [Fig. 2(a2) and Fig. 2(b2)]. Comparisons with

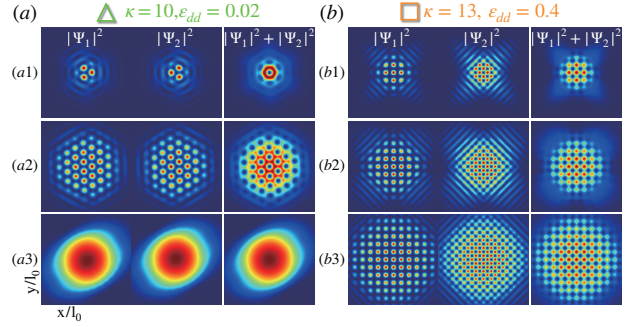


FIG. 2. Density profiles and spin textures of (a) meron-type and (b) skyrmion-type CSSs are shown for varying intra- and inter-component contact interactions. The interaction strengths are (a1,b1)  $g_{ij}N = g_{ii}N = 0.5$ , (a2,b2)  $g_{ij}N = 0.5$ ,  $g_{ii}N = 20$ , and (a3,b3)  $g_{ij}N = 10$ ,  $g_{ii}N = 0.5$ .

contact-only systems [61] highlight the essential role of dipolar repulsion in sustaining these hybrid phases. Under strong intra-component interactions ( $g_{ii}N = 10$ ), the system undergoes a transition from homogeneous superfluidity ( $\kappa < \kappa_c$ ) to chiral supersolidity ( $\kappa \geq \kappa'_c$ ), with strong SOC and DDI ( $\kappa = 13$ ,  $\varepsilon_{dd} = 0.4$ ) stabilizing a square lattice [Fig. 2(a3) and Fig. 2(b3)]. These results demonstrate the dual role of interactions in structuring density and spin degrees of freedom, enabling the design of chiral spin supersolids in spinor dipolar condensates.

*Crystalline order and non-classical rotational inertia fraction.*—To distinguish the crystalline properties of CSS from the superfluidity of the singly skyrmion phase, we employ two key observables: crystalline order, quantifying density modulation [62, 63], and the NCRIF, a measure of supersolidity [64]. As shown in Fig. 1(b3) and Fig. 1(b4), both crystalline order and NCRIF identify the transition from singly skyrmion superfluidity to meron supersolidity. Similarly, NCRIF exhibits significant variation between meron and skyrmion supersolids, underscoring its sensitivity to changes in lattice symmetry and superfluid fraction.

The crystalline order  $C = \frac{\rho_{\max}(\mathbf{k}) - \rho_{\min}(\mathbf{k})}{\rho_{\max}(\mathbf{k}) + \rho_{\min}(\mathbf{k})}$  quantifies density modulation in momentum space, where  $\rho_{\max}(\mathbf{k})$  and  $\rho_{\min}(\mathbf{k})$  are the maximum and minimum densities on the Rashba ring, respectively. For the meron lattice,  $C$  jumps abruptly from 0.03 to 1 at  $\kappa_c \approx 9$  [Fig. 1(b3)], signaling a first-order transition from superfluid to chiral meron supersolid. This aligns with the NCRIF results, confirming the first-order nature of the transition.

To characterize the transition between CSSs, we evaluate the NCRIF, defined as

$$f_{\text{NCRI}} = \frac{\rho_s}{\rho_0} = \frac{1}{\langle \frac{1}{\rho_s(r)} \rangle \langle \rho(r) \rangle}, \quad (2)$$

where  $\rho(r) = \int d\varphi \rho(\mathbf{r}, \varphi) / 2\pi$  and  $\rho_s(r) = 2\pi / \int d\varphi \rho^{-1}(\mathbf{r}, \varphi)$  are the total and superfluid densities, respectively [65, 66]. Here,  $f_{\text{NCRI}} = 1$  (0) corresponds to

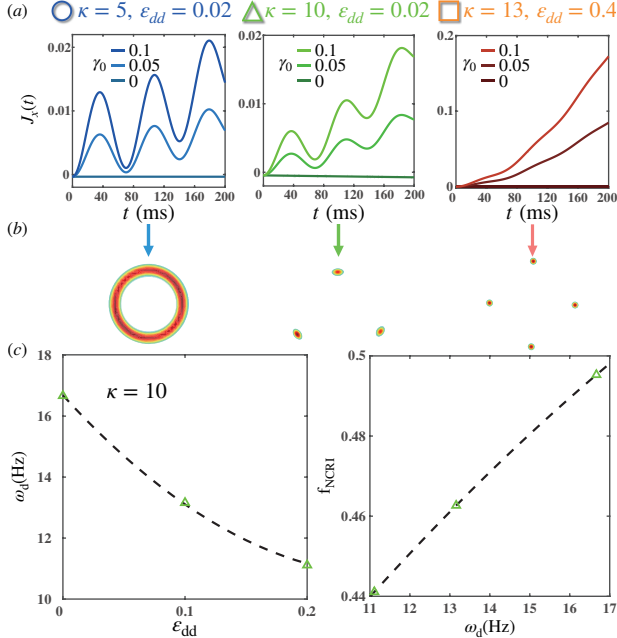


FIG. 3. (a) Current dynamics  $J_x(t)$  for the phases labeled in Fig. 1(a). (b) Density profiles in momentum space reveal the breaking of continuous rotational symmetry into 3- or 4-fold discrete rotational symmetries for triangular and square lattices, respectively. (c) Non-equilibrium oscillation frequency versus DDI strength and NCRIF.

a pure superfluid (solid), while  $0 < f_{\text{NCRI}} < 1$  indicates supersolidity. As shown in Fig. 1(b4), the NCRIF drops discontinuously from 0.9 to 0.4 at  $\kappa_c \approx 9$ , confirming a first-order transition from superfluid to chiral meron supersolid, consistent with the crystalline order results.

Fig. 1(b1) and Fig. 1(b2) show the crystalline order and NCRIF across the transition from superfluid to skyrmion supersolid. Their continuous variation indicates a second-order transition, controlled by the SOC strength in the presence of strong dipolar interactions. As seen in Fig. 3(b), the modulated state comprises two pairs of orthogonal wavenumbers. Expanding energy of the system in terms of the modulation amplitude reveals a vanishing cubic term due to wavenumber orthogonality, explaining the second-order transition to a skyrmion square lattice [43]. Increasing SOC reduces the NCRIF below 1, confirming crystallization into a supersolid. This second-order transition reflects gradual energy redistribution, consistent with the continuous evolution of the superfluid fraction.

*Non-equilibrium driven-oscillation.*—To probe supersolidity-dissipation interplay, we introduce  $\mathcal{PT}$ -symmetric dissipation [67–70] into a quasi-2D system. The non-Hermitian dissipation Hamiltonian is [71]

$$\mathcal{H}_{\text{diss}} = -i\hbar \int d\mathbf{r} \gamma(\mathbf{r}) \sum_{j=1,2} |\Psi_j|^2, \quad (3)$$

where  $\gamma(\mathbf{r}) = \gamma_R(\mathbf{r}) - \gamma_L(\mathbf{r})$  is the localized dissipation rate with  $\gamma_l(\mathbf{r}) = \gamma_0 \exp\left[-\frac{(x-x_l)^2+(y-y_l)^2}{2\sigma^2}\right]$  for  $l = L, R$  [72–74]. Here,  $\sigma = 0.1$  and  $\gamma_0$  are the dissipation width and amplitude, respectively, with gain and loss localized at  $x_{R,L} = \pm 0.8$  and  $y_l = 0$ . This drives a current

$$\mathbf{J}(t) = -\frac{i}{2} \int d\mathbf{r} \sum_{j=1,2} (\Psi_j^* \nabla \Psi_j - \Psi_j \nabla \Psi_j^*). \quad (4)$$

linking equilibrium superfluid fractions to non-equilibrium dynamics (Fig. 3).

The current dynamics  $J_x(t)$  and driven-oscillation frequency  $\omega_d$  versus dipolar interaction strength (Fig. 3) align with recent experiments probing supersolidity via non-equilibrium dynamics [75]. Unlike closed-system experiments, our open-system framework reveals how lattice symmetry and superfluid fraction, key signatures of supersolidity, govern dissipation-driven responses.

In the singly skyrmion superfluid phase, undamped  $J_x(t)$  oscillations [Fig. 3(a)] reflect global phase coherence [76], yielding a near-unity superfluid fraction ( $f_{\text{NCRI}} \approx 1$ ). In the meron supersolid phase, partial damping arises from triangular lattice rigidity and fragmented superflow, reducing  $f_{\text{NCRI}}$  to 0.4. For the skyrmion supersolid, rapid suppression of  $J_x(t)$  oscillations reveals square lattice-induced superfluid fragmentation, with  $f_{\text{NCRI}} = 0.5$ . These results highlight the role of lattice symmetry in governing superfluid coherence and dissipation.

Fig. 3 bridges equilibrium phase transitions (Fig. 1) and non-equilibrium dynamics, linking current responses to the superfluid fraction. The oscillation frequency [Fig. 3(c)] versus  $f_{\text{NCRI}}$  provides a quantitative probe of supersolidity, validated by experiments [75]. These results align with recent advances [75, 77], highlighting supersolids as hybrid quantum systems where crystalline order and superfluidity coexist and compete.

*Experimental implementation.*—The proposed system can be realized using magnetic atoms (e.g.,  $^{52}\text{Cr}$ ,  $^{164}\text{Dy}$ , or  $^{168}\text{Er}$ ) in a crossed optical dipole trap. We select the two lowest Zeeman sublevels,  $|1\rangle = |m_J = -J\rangle$  and  $|2\rangle = |m_J = 0\rangle$ , to engineer a spin-1/2 spin-orbit coupled system with coexisting dipolar and non-dipolar components [48, 49]. A laser-induced quadratic Zeeman shift [79] drives atoms to these states while suppressing dipolar relaxation [80, 81]. The sublevels are coupled via optical Raman dressing, as demonstrated in recent experiments [82]. Contact and dipolar interactions are tunable via Feshbach resonances [83] and polarization rotation [84], respectively, while SOC is controlled via Raman dressing [35, 44–46]. The quasi-2D condensate is achieved by strong harmonic confinement  $V(\mathbf{r}) = M(\omega_\perp^2 \mathbf{r}^2 + \omega_z^2 z^2)/2$  with  $\omega_z \gg \omega_\perp$ .

*Conclusions.*—We demonstrate chiral supersolid phases in a two-dimensional spin-orbit coupled dipolar BEC, where crystalline order coexists with tunable spin

textures and non-equilibrium dynamics. By engineering dipolar interactions and Rashba SOC, we uncover two quantum phase transitions: a first-order transition to a triangular lattice of meron-antimeron pairs and a second-order transition to a square skyrmion lattice. These transitions arise from competing dipolar and SOC energies, with the latter possessing a non-Abelian feature for hosting chiral spin textures. The coexistence of supersolidity and topology resolves a key challenge in quantum gas research. Experimental protocols using magnetic atoms, including optical Raman dressing for SOC and Feshbach tuning for interaction control, validate feasibility. Non-equilibrium dynamics under  $\mathcal{PT}$ -symmetric dissipation link oscillation currents to the superfluid fraction, providing a novel probe for supersolidity.

This work bridges quantum simulation and topological phase transitions in condensed matter systems, establishing dipolar quantum gases as a versatile platform for engineering topological spin textures. Our results open avenues for exploring topological quantum matter and dissipation-driven control. Future studies on excitation spectra [85–87], quantum fluctuations [88], and hybrid quantum states could advance applications in spintronics and topological quantum computing [89, 90].

*Acknowledgments.*—We thank H. Saito and L. Vernac for helpful discussions. This work was supported by National Key Research and Development Program of China (2021YFA1401700), NSF of China (Grants No. 11847237 and 12104359), Shaanxi Academy of Fundamental Sciences (Mathematics, Physics) (Grant No. 22JSY036), and Shaanxi Fundamental Science Research Project for Mathematics and Physics (Grant No. 23JSQ015), and the Fundamental Research Funds for the Central Universities (xpt012024033). Y.C.Z. acknowledges the support of Xi'an Jiaotong University through the “Young Top Talents Support Plan” and Basic Research Funding.

- 
- \* xfzhang@sust.edu.cn  
 † wliu@iphy.ac.cn  
 ‡ zhangyc@xjtu.edu.cn
- [1] M. Kuepferling, A. Casiraghi, G. Soares, G. Durin, F. Garcia-Sanchez, L. Chen, C. H. Back, C. H. Marrows, S. Tacchi, and G. Carlotti, Rev. Mod. Phys. **95**, 015003 (2023).
  - [2] J. Junquera, Y. Nahas, S. Prokhorenko, L. Bellaiche, J. Íñiguez, D. G. Schlom, L.-Q. Chen, S. Salahuddin, D. A. Muller, L. W. Martin, and R. Ramesh, Rev. Mod. Phys. **95**, 025001 (2023).
  - [3] S. A. Yang, H. Pan, and F. Zhang, Phys. Rev. Lett. **115**, 156603 (2015).
  - [4] T. D. Lee and C. N. Yang, Phys. Rev. **104**, 254 (1956).
  - [5] E. Nakano and T. Tatsumi, Phys. Rev. D **71**, 114006 (2005).
  - [6] D. A. Allwood, G. Xiong, C. C. Faulkner, D. Atkinson, D. Petit, and R. P. Cowburn, Science **309**, 1688 (2005).
  - [7] S. S. P. Parkin, M. Hayashi, and L. Thomas, Science **320**, 190 (2008).
  - [8] S. Woo, K. Litzius, B. Krüger, M.-Y. Im, L. Caretta, K. Richter, M. Mann, A. Krone, R. M. Reeve, M. Weigand, P. Agrawal, I. Lemesh, M.-A. Mawass, P. Fischer, M. Kläui, and G. S. D. Beach, Nat. Mater. **15**, 501 (2016).
  - [9] A. Fert, V. Cros, and J. Sampaio, Nat. Nanotechnol. **8**, 152 (2013).
  - [10] N. Romming, C. Hanneken, M. Menzel, J. E. Bickel, B. Wolter, K. von Bergmann, A. Kubetzka, and R. Wiesendanger, Science **341**, 636 (2013).
  - [11] J. Sampaio, V. Cros, S. Rohart, A. Thiaville, and A. Fert, Nat. Nanotechnol. **8**, 839 (2013).
  - [12] N. Nagaosa and Y. Tokura, Nat. Nanotechnol. **8**, 899 (2013).
  - [13] W. Kang, Y. Huang, X. Zhang, Y. Zhou, and W. Zhao, Proc. IEEE **104**, 2040 (2016).
  - [14] A. Fert, N. Reyren, and V. Cros, Nat. Rev. Mater. **2**, 17031 (2017).
  - [15] R. Takagi, J. S. White, S. Hayami, R. Arita, D. Honecker, H. M. Rønnow, Y. Tokura, and S. Seki, Sci. Adv. **4**, eaau3402 (2018).
  - [16] C. Kittel, *Introduction to Solid State Physics* (Wiley, New York, 2005).
  - [17] X. Z. Yu, Y. Onose, N. Kanazawa, J. H. Park, J. H. Han, Y. Matsui, N. Nagaosa, and Y. Tokura, Nature (London) **465**, 901 (2010).
  - [18] S. Mühlbauer, B. Binz, F. Jonietz, C. Pfleiderer, A. Rosch, A. Neubauer, R. Georgii, and P. Böni, Science **323**, 915 (2009).
  - [19] X. Z. Yu, N. Kanazawa, Y. Onose, K. Kimoto, W. Z. Zhang, S. Ishiwata, Y. Matsui, and Y. Tokura, Nat. Mater. **10**, 106 (2011).
  - [20] S. Seki, X. Z. Yu, S. Ishiwata, and Y. Tokura, Science **336**, 198 (2012).
  - [21] Y. Tokunaga, X. Z. Yu, J. S. White, H. M. Rønnow, D. Morikawa, Y. Taguchi, and Y. Tokura, Nat. Commun. **6**, 7638 (2015).
  - [22] Y.-X. Hu, C. Miniatura, and B. Grémaud, Phys. Rev. A **92**, 033615 (2015).
  - [23] S.-Z. Lin, A. Saxena, and C. D. Batista, Phys. Rev. B **91**, 224407 (2015).
  - [24] S. D. Yi, S. Onoda, N. Nagaosa, and J. H. Han, Phys. Rev. B **80**, 054416 (2009).
  - [25] T. Kurumaji, T. Nakajima, V. Ukleev, A. Feoktystov, T. Arima, K. Kakurai, and Y. Tokura, Phys. Rev. Lett. **119**, 237201 (2017).
  - [26] X. Z. Yu, W. Koshibae, Y. Tokunaga, K. Shibata, Y. Taguchi, N. Nagaosa, and Y. Tokura, Nature (London) **564**, 95 (2018).
  - [27] M. Erol-Kantarci and H. T. Mouftah, IEEE Commun. Surv. Tutorials **17**, 179 (2015).
  - [28] M. Filianina, J.-P. Hanke, K. Lee, D.-S. Han, S. Jaiswal, A. Rajan, G. Jakob, Y. Mokrousov, and M. Kläui, Phys. Rev. Lett. **124**, 217701 (2020).
  - [29] F. Böttcher, J.-N. Schmidt, J. Hertkorn, K. S. H. Ng, S. D. Graham, M. Guo, T. Langen, and T. Pfau, Rep. Prog. Phys. **84**, 012403 (2021).
  - [30] M. A. Norcia and F. Ferlaino, Nat. Phys. **17**, 1349 (2021).
  - [31] L. Chomaz, I. Ferrier-Barbut, F. Ferlaino, B. Laburthe-Tolra, B. L. Lev, and T. Pfau, Rep. Prog. Phys. **86**, 026401 (2023).
  - [32] N. Defenu, T. Donner, T. Macrì, G. Pagano, S. Ruffo,

- and A. Trombettoni, Rev. Mod. Phys. **95**, 035002 (2023).
- [33] A. Recati and S. Stringari, Nat. Rev. Phys. **5**, 735 (2023).
- [34] S. Gopalakrishnan, I. Martin, and E. A. Demler, Phys. Rev. Lett. **111**, 185304 (2013).
- [35] Y. Deng, J. Cheng, H. Jing, C.-P. Sun, and S. Yi, Phys. Rev. Lett. **108**, 125301 (2012).
- [36] Q. Zhou and X. Cui, Phys. Rev. Lett. **110**, 140407 (2013).
- [37] Y. Li, Y. Liu, Z. Fan, W. Pang, S. Fu, and B. A. Malomed, Phys. Rev. A **95**, 063613 (2017).
- [38] R. Liao, Phys. Rev. Lett. **120**, 140403 (2018).
- [39] W. Han, X.-F. Zhang, D.-S. Wang, H.-F. Jiang, W. Zhang, and S.-G. Zhang, Phys. Rev. Lett. **121**, 030404 (2018).
- [40] K. T. Geier, G. I. Martone, P. Hauke, and S. Stringari, Phys. Rev. Lett. **127**, 115301 (2021).
- [41] K. T. Geier, G. I. Martone, P. Hauke, W. Ketterle, and S. Stringari, Phys. Rev. Lett. **130**, 156001 (2023).
- [42] M. A. Baranov, M. Dalmonte, G. Pupillo, and P. Zoller, Chem. Rev. **112**, 5012 (2012).
- [43] Y.-C. Zhang and F. Maucher, Atoms **11**, 102 (2023).
- [44] K. Jiménez-García, L. J. LeBlanc, R. A. Williams, M. C. Beeler, C. Qu, M. Gong, C. Zhang, and I. B. Spielman, Phys. Rev. Lett. **114**, 125301 (2015).
- [45] N. Q. Burdick, Y. Tang, and B. L. Lev, Phys. Rev. X **6**, 031022 (2016).
- [46] See Supplemental Material for more details on the experimental implementation of our proposal.
- [47] C. Chin, R. Grimm, P. S. Julienne, and E. Tiesinga, Rev. Mod. Phys. **82**, 1225 (2010).
- [48] H. Saito, Y. Kawaguchi, and M. Ueda, Phys. Rev. Lett. **102**, 230403 (2009).
- [49] W. E. Shirley, B. M. Anderson, C. W. Clark, and R. M. Wilson, Phys. Rev. Lett. **113**, 165301 (2014).
- [50] B. Dong, Q. Sun, W.-M. Liu, A.-C. Ji, X.-F. Zhang, and S.-G. Zhang, Phys. Rev. A **96**, 013619 (2017).
- [51] C. J. Pethick and H. Smith, *Bose-Einstein Condensation in Dilute Gases* (Cambridge University Press, Cambridge, 2002).
- [52] L. Pitaevskii and S. Stringari, *Bose-Einstein Condensation and Superfluidity* (Oxford University Press, Oxford, 2016).
- [53] T. D. Lee and C. N. Yang, Phys. Rev. **105**, 1119 (1957).
- [54] T. D. Lee, K. Huang, and C. N. Yang, Phys. Rev. **106**, 1135 (1957).
- [55] We would like to point out that the Lee-Huang-Yang (LHY) correction [53, 54] has been omitted in our theory Eq. (1), since the following discussion is focused on the weak dipolar interaction case. In such condition, the LHY effect is reasonably negligible which has been verified numerically.
- [56] H. Hu, B. Ramachandhran, H. Pu, and X.-J. Liu, Phys. Rev. Lett. **108**, 010402 (2012).
- [57] G. Juzeliūnas, J. Ruseckas, and J. Dalibard, Phys. Rev. A **81**, 053403 (2010).
- [58] C.-J. Wu, I. Mondragon-Shem, and X.-F. Zhou, Chin. Phys. Lett. **28**, 097102 (2011).
- [59] R. Liao, O. Fialko, J. Brand, and U. Zülicke, Phys. Rev. A **92**, 043633 (2015).
- [60] S. Heinze, K. von Bergmann, M. Menzel, J. Brede, A. Kubetzka, R. Wiesendanger, G. Bihlmayer, and S. Blügel, Nat. Phys. **7**, 713 (2011).
- [61] S. Sinha, R. Nath, and L. Santos, Phys. Rev. Lett. **107**, 270401 (2011).
- [62] Y.-C. Zhang, F. Maucher, and T. Pohl, Phys. Rev. Lett. **123**, 015301 (2019).
- [63] E. Poli, T. Bland, S. J. M. White, M. J. Mark, F. Ferlaino, S. Trabucco, and M. Mannarelli, Phys. Rev. Lett. **131**, 223401 (2023).
- [64] L. Tanzi, J. G. Maloberti, G. Biagioni, A. Fioretti, G. Gabbanini, and G. Modugno, Science **371**, 1162 (2021).
- [65] A. J. Leggett, Phys. Rev. Lett. **25**, 1543 (1970).
- [66] N. Henkel, F. Cinti, P. Jain, G. Pupillo, and T. Pohl, Phys. Rev. Lett. **108**, 265301 (2012).
- [67] C. M. Bender and S. Boettcher, Phys. Rev. Lett. **80**, 5243 (1998).
- [68] Y.-M. Hu, H.-Y. Wang, Z. Wang, and F. Song, Phys. Rev. Lett. **132**, 050402 (2024).
- [69] V. V. Konotop, J. Yang, and D. A. Zezyulin, Rev. Mod. Phys. **88**, 035002 (2016).
- [70] C. M. Bender and D. W. Hook, Rev. Mod. Phys. **96**, 045002 (2024).
- [71] L. Pan, X. Chen, Y. Chen, and H. Zhai, Nat. Phys. **16**, 767 (2020).
- [72] V. A. Brazhnyi, V. V. Konotop, V. M. Pérez-García, and H. Ott, Phys. Rev. Lett. **102**, 144101 (2009).
- [73] G. Barontini, R. Labouvie, F. Stubenrauch, A. Vogler, V. Guarnera, and H. Ott, Phys. Rev. Lett. **110**, 035302 (2013).
- [74] R. Labouvie, B. Santra, S. Heun, and H. Ott, Phys. Rev. Lett. **116**, 235302 (2016).
- [75] G. Biagioni, N. Antolini, B. Donelli, L. Pezzè, A. Smerzi, M. Fattori, A. Fioretti, C. Gabbanini, M. Inguscio, L. Tanzi, and G. Modugno, Nature (London) **629**, 773 (2024).
- [76] J. Williams, R. Walser, J. Cooper, E. Cornell, and M. Holland, Phys. Rev. A **59**, R31 (1999).
- [77] E. Zhao, Z. Wang, C. He, Ting Fung Jeffrey Poon, K. K. Pak, Y.-J. Liu, P. Ren, X.-J. Liu, and G.-B. Jo, Nature (London) **637**, 565 (2025).
- [78] B. M. Garraway and V. G. Minogin, Phys. Rev. A **62**, 043406 (2000).
- [79] L. Santos, M. Fattori, J. Stuhler, and T. Pfau, Phys. Rev. A **75**, 053606 (2007).
- [80] A. Griesmaier, J. Stuhler, and T. Pfau, Appl. Phys. B **82**, 211 (2006).
- [81] B. Pasquiou, G. Bismut, Q. Beaufils, A. Crubellier, E. Maréchal, P. Pedri, L. Vernac, O. Gorceix, and B. Laburthe-Tolra, Phys. Rev. A **81**, 042716 (2010).
- [82] M. Lecomte, A. Journeaux, J. Veschambre, J. Dalibard, and R. Lopes, Phys. Rev. Lett. **134**, 013402 (2025).
- [83] T. Lahaye, T. Koch, B. Fröhlich, M. Fattori, J. Metz, A. Griesmaier, S. Giovanazzi, and T. Pfau, Nature (London) **448**, 672 (2007).
- [84] S. Giovanazzi, A. Görlitz, and T. Pfau, Phys. Rev. Lett. **89**, 130401 (2002).
- [85] P. B. Blakie, Phys. Rev. Lett. **134**, 013401 (2025).
- [86] S. Lepoutre, A. Journeaux, J. Veschambre, J. Dalibard, and R. Lopes, Phys. Rev. A **111**, 033310 (2025).
- [87] L. M. Platt, D. Baillie, and P. B. Blakie, arXiv:2412.15552.
- [88] B. Donelli, N. Antolini, G. Biagioni, M. Fattori, A. Fioretti, C. Gabbanini, M. Inguscio, L. Tanzi, G. Modugno, A. Smerzi, and L. Pezzè, arXiv:2501.17142.
- [89] A. P. Petrović, C. Psaroudaki, P. Fischer, M. Garst, and C. Panagopoulos, arXiv:2410.11427.
- [90] S. L. Cornish, M. R. Tarbutt, and K. R. A. Hazzard, Nat. Phys. **20**, 730 (2024).